The Astrophysical Journal Supplement Series, 260:56 (9pp), 2022 June https://doi.org/10.3847/1538-4365/ac721a

Experimental and Theoretical Radiative Parameters of Highly Excited Odd-parity Levels in Ir II

Huiting Ma[1], Meina Liu[1], Yidan Geng[1], Ting Wang[1], Ziqing Yu[1], Hongfeng Zheng[1], Sébastien Gamrath[2], Pascal Quinet[2,3], and Zhenwen Dai[1]

[1] Key Laboratory of Physics and Technology for Advanced Batteries (Ministry of Education), College of Physics, Jilin University, Changchun 130012, People's Republic of China; dai@jlu.edu.cn
[2] Physique Atomique et Astrophysique, Université de Mons, B-7000 Mons, Belgium; pascal.quinet@umons.ac.be
[3] IPNAS, Université de Liège, B-4000 Liège, Belgium
Received 2022 January 11; revised 2022 May 18; accepted 2022 May 19; published 2022 July 6

Abstract

Using the time-resolved laser-induced fluorescence technique, the radiative lifetimes for 15 odd-parity levels from 47,003 to 61,475 cm^{-1} in Ir II were measured. To the best of our knowledge, 11 lifetime results among these levels are reported for the first time, and hence they should be a good complement to the measured lifetime data of 10 levels previously published in the literature. The pseudorelativistic Hartree–Fock including core-polarization corrections method was used to calculate the lifetimes and branching fractions (BFs) of the investigated energy levels. Combining the experimental lifetime with the theoretical BFs, the transition probabilities and oscillator strengths for 124 transitions were determined.

Unified Astronomy Thesaurus concepts: Atomic spectroscopy (2099); Atomic physics (2063); Transition probabilities (2074); Radiative processes (2055)

1. Introduction

In recent decades, high-resolution near-ultraviolet spectra from the Hubble Space Telescope were used to detect the third rapid neutron-capture (r-process) peak elements (osmium, iridium, and platinum) in r-process-enriched stars such as some metal-poor (MP) halo stars and chemically peculiar (CP) stars (Cowan et al. 1996; Sneden et al. 1998; Roederer & Lawler 2012). The abundances of these heavy elements provide valuable information about the conditions for the formation of these elements in supernovae and merging neutron stars (Roederer & Lawler 2012), and they also play an important role in understanding the atmospheric processes that lead to anomalies in the spectra of CP stars (Ivarsson et al. 2004). Moreover, these elements are more desirable for age dating of the oldest stars than the lighter elements (Frebel 2018). The radiative parameters (including transition probabilities and oscillator strengths etc.) of atoms and ions of these heavy elements are of course vital for the determination of elemental abundances. A reliable and convenient method to obtain oscillator strengths is through the combination of measured radiative lifetimes with reliable branching fractions (BFs).

Iridium ($Z = 77$), as a heavy element predominantly formed by the r-process, is observed in its singly ionized form in many stars, e.g., the CP star χ Lupi (Ivarsson et al. 2004), the MP halo star HD 160617 (Roederer et al. 2012), the A1 Vm star Sirius (Cowley et al. 2016), and the hot Am star HR 3383 (Wahlgren et al. 2021) etc. Ivarsson et al. (2004) used the time-resolved laser-induced fluorescence (TR-LIF) technique to measure the radiative lifetimes for nine odd-parity levels of Ir II, and combined with BFs determined by Fourier transform spectroscopic measurement, obtained the oscillator strengths and transition probabilities of 23 transitions of Ir II. Based on these data, they determined the abundance of iridium in the CP star χ Lupi. Xu et al. (2007) measured lifetimes of four odd-parity Ir II levels using the TR-LIF technique, and calculated the lifetimes and BFs of 21 Ir II levels with the pseudorelativistic Hartree–Fock method including core-polarization corrections (HFR+CPOL) method. Combining the experimental lifetime values of 10 energy levels from their work and from Ivarsson et al. (2004) with theoretical BFs, the semiempirical transition probabilities for 93 transitions were obtained. In addition, they also calculated the theoretical transition probabilities for other 11 energy levels.

Among the 76 energy levels of Ir II included in the NIST Atomic Spectroscopy Database (Kramida et al. 2020), the experimental lifetimes of a total of 10 levels in the energy range 44,575.66–52,510.1 cm^{-1} have been published so far, as far as we know. In this work, the radiative lifetimes of the 15 highly excited levels ranging from 47,003 to 61,475 cm^{-1} are measured by the TR-LIF technique, including four levels for which the experimental lifetimes have also been reported in the literature. In addition, the new radiative lifetime data obtained in this work were combined with BFs obtained from HFR +CPOL to deduce semiempirical transition probabilities and oscillator strengths for 124 Ir II spectral lines.

2. Lifetime Measurements

An approach widely used for lifetime measurements is the TR-LIF technique. This method has several advantages. In view of the selective excitation, no cascading problems arising from the higher-lying levels are present. In addition, a large number of levels are accessible through the use of one-step one-photon, one-step two-photon, and two-step excitations (Biémont & Quinet 2003). The experimental setup used in this work is similar to that described in the paper by Tian et al. (2016), so only a brief outline is given here.

A 532 nm Nd:YAG pulsed laser with a repetition frequency of 10 Hz, pulse energy of 5–10 mJ, and a pulse width of about

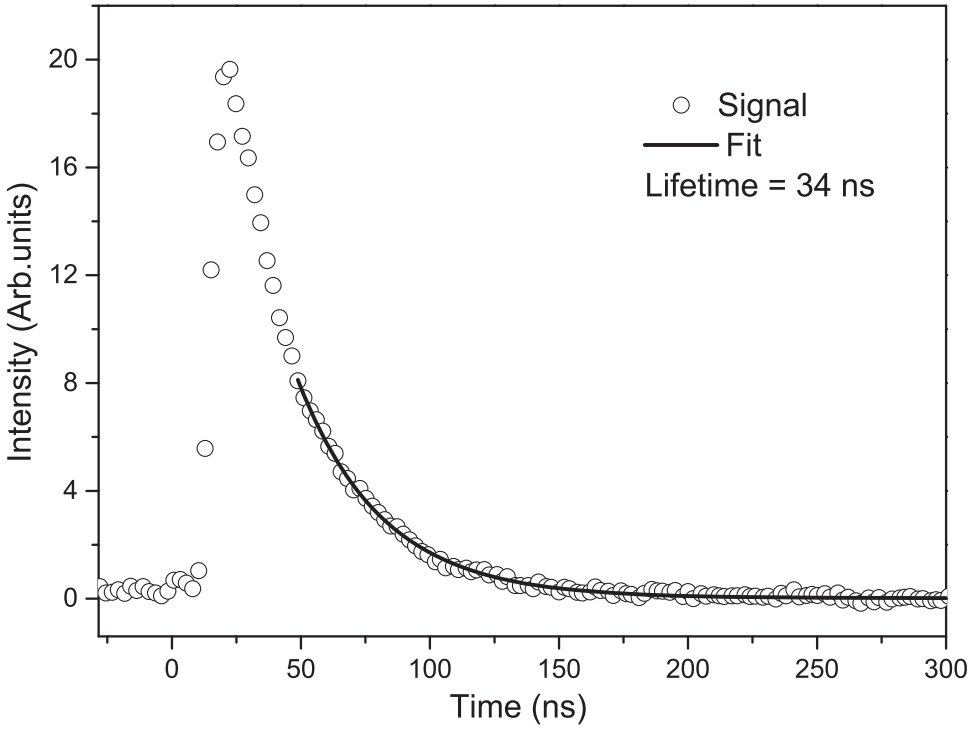

Figure 1. A typical fluorescence decay curve of the Ir II 50,302.01 cm^{-1} level with an exponential fit.

8 ns was used as the ablation laser to focus onto a rotating iridium target inside a vacuum chamber to produce laser plasma containing free singly ionized iridium ions at ground and lower-lying metastable levels. Another Nd:YAG laser, with the same performance parameters except for pulse energy, was sent to a temporal compressor which was based on the stimulated Brillouin scattering technique in water to compress the pulse width to about 2 ns. These compressed pulses were used to pump a dye laser (Sirah Cobra-stretch) with Rhodamine 640, DCM, or Rhodamine 6G dyes, and a tunable laser at 611–662, 604–658, or 558–588 nm was obtained. In order to obtain the desired excitation wavelength (205–288 nm), two methods of frequency conversion were employed. One is the frequency doubling or tripling of the dye laser produced by one or two β-barium borate type-I crystals. The other is the first- or second-order Stokes components by stimulated Raman scattering in a H_2 gas cell using the frequency-doubled or frequency-tripled dye laser. A digital delay generator (SRS DG535) was used to adjust the delay between the excitation laser and the ablation laser. To obtain an accurate excitation wavelength, the excitation laser was monitored by a high-precision wavelength meter (HighFinesse WS6). In the vacuum chamber, the ablation laser was focused vertically on the iridium target and the excitation laser horizontally passed through the iridium plasma region about 8 mm above the target to excite the levels of interest. In the direction orthogonal to both the ablation and excitation laser beams, the laser-induced fluorescence from the investigated upper level was collected by a fused-silica lens, filtered by a monochromator, and finally detected by a microchannel plate photomultiplier tube (PMT) (Hamamatsu R3809U-58). The line width of the monochromator is 15 nm when its slit width is 3 mm, which can eliminate the effect of possible cascade fluorescence from lower levels. A 1 GHz digital oscilloscope (Keysight DSOX3102T) registered and averaged the time-resolved photocurrent signal from the PMT. In addition, in order to eliminate the Zeeman quantum-beat effect from the Earth's magnetic field and at the same time weaken the background of plasma recombination processes, a magnetic field of about 100 G produced by a pair of Helmholtz coils was applied to the plasma zone.

In the experiment, the fluorescence signal intensity is proportional to the number of photons emitted per unit time, and the latter is proportional to the particle density at an excited state, so the fluorescence intensity directly reflects the change of excited-state particle number density over time. For a decay curve with longer lifetime, an exponential fit to the portion where the exciting pulse and its stray light ceased can determine the decay constant. For a decay curve with a shorter lifetime, the portion in the curve without interference of the excitation laser but with a good signal-to-noise ratio is almost nonexistent, and hence a convolution fit to the curve is needed to be performed by a combination with a recorded excitation pulse (Li et al. 1999). The uncertainties of lifetime results obtained from the fits are not related to whether a convolution fit or an e-exponential fit is used, but to the signal-to-noise ratios of fluorescence curves. Figure 1 shows the fluorescence decay curve observed at 237 nm from the 50,302.01 to 2262.84 cm^{-1} levels, which was fitted with an exponential. In addition, a typical fluorescence decay curve of the 55,852.50 cm^{-1} level with the fitted convolution curve of a laser pulse and an exponential is shown in Figure 2.

3. Theoretical Calculations

In combination with the experimental lifetime measurements performed in this work, we also considered atomic data calculated from a theoretical model based on the HFR+CPOL method of Cowan (1981), as described, e.g., by Quinet et al. (1999, 2002) and Quinet (2017). More precisely, the same physical model as the one used by Xu et al. (2007) was

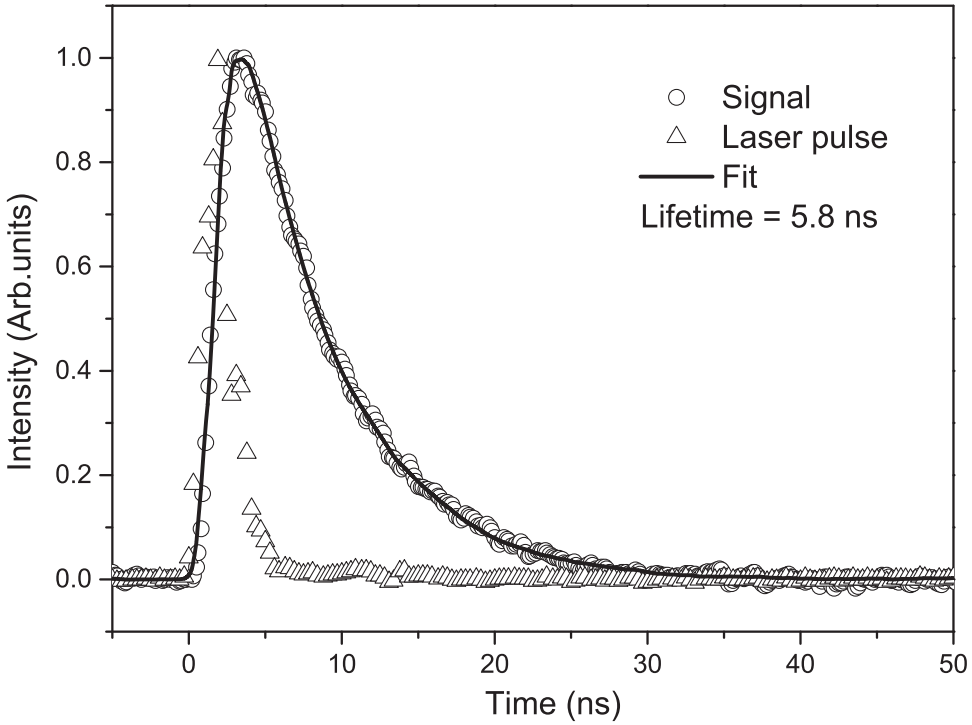

Figure 2. A typical fluorescence decay curve of the Ir II 55,852.50 cm^{-1} level with the fitted convolution curve between the laser pulse and an exponential.

Table 1
Measured and Calculated Lifetimes of Ir II Highly Excited Levels and Comparison with Previous Results

Upper Level[a]		Lower Level[a]		$\lambda_{Exc.}$ (nm)	$\lambda_{Obs.}$ (nm)	Lifetime (ns)			
Assignment	Energy (cm^{-1})	J	Energy (cm^{-1})			Exp.	Cal.		Previous Exp.
							HFR	HFR +CPOL	
$5d^7(^4F_{9/2})6p$ $(9/2,1/2)^\circ_5$	47,003.95	5	0	212.748	224	4.1(3)	2.8	3.9	4.4 (3)[b],4.3(4)[c]
$5d^6 6s(^6D_{9/2})6p$ $(9/2,1/2)^\circ_4$	50,302.01	4	2262.84	208.163	237	34(3)	27	38	34(3)[b]
$5d^6 6s(^6D_{9/2})6p$ $(9/2,1/2)^\circ_5$	51,333.00	4	4787.92	214.845	253	53(3)	44	63	52.0(5)[b]
$5d^7(^4P_{5/2})6p$ $(5/2,1/2)^\circ_2$	51,371.97	2	3090.16	207.117	207	6.6(4)	4.2	5.8	6.6(5)[b]
$5d^7(^4F_{3/2})6p(3/2,1/2)^\circ_2$	53,678.68	2	18,944.91	287.904	301	6.3(10)	5.0	6.9	
$5d^7(^4F_{9/2})6p$ $(9/2,3/2)^\circ_5$	53,691.38	4	4787.92	204.485	291	3.4(3)	2.2	3.1	
$5d^7(^4F_{5/2})6p$ $(5/2,1/2)^\circ_3$	55,852.50	3	8186.89	209.795	225	5.8(3)	5.2	7.2	
$5d^7(^4F_{9/2})6p$ $(9/2,3/2)^\circ_4$	56,233.93	3	8186.89	208.129	278	3.3(2)	2.9	4.0	
$5d^7(^4P_{3/2})6p$ $(3/2,1/2)^\circ_1$	56,241.53	2	8974.95	211.566	223	8.5(4)	4.8	6.6	
$5d^6 6s(^6D_{5/2})6p$ $(5/2,1/2)^\circ_2$	56,354.21	3	8186.89	207.610	225	9.3(3)	7.0	9.8	
5664°_2	56,644.46	2	8974.95	209.778	224	4.6(4)	3.2	4.4	
$5d^7(^4P_{1/2})6p$ $(1/2,1/2)^\circ_0$	56,875.79	1	9062.22	209.146	224	5.5(3)	3.6	5.0	
$5d^7(^4P_{3/2})6p$ $(3/2,1/2)^\circ_2$	59,132.98	2	11,307.53	209.094	215	5.9(3)	4.5	6.3	
$5d^7(^4F_{9/2})6p$ $(9/2,3/2)^\circ_3$	60,313.63	4	11,719.11	205.785	259	3.4(3)	3.2	4.4	
6147°_3	61,474.19	3	12,714.66	205.088	334	3.9(3)	3.0	4.1	

Notes.
[a] Kramida et al. (2020).
[b] Ivarsson et al. (2004).
[c] Xu et al. (2007).

considered in the present study, namely by incorporating the $5d^76s$, $5d^77s$, $5d^76d$, $5d^66s^2$, $5d^66p^2$, $5d^66s7s$, $5d^66s6d$, $5d^56s^27s$, $5d^56s^26d$, and $5d^8$ even-parity configurations, and the $5d^76p$, $5d^77p$, $5d^75f$, $5d^66s6p$, $5d^66s7p$, $5d^66s5f$, and $5d^56s^26p$ odd-parity configurations. The core-polarization effects corresponding to a Ta-like ionic core were considered using the dipole polarizabilty of Ir V (Fraga et al. 1976), i.e., $\alpha_d = 4.59$ au, and a cutoff radius, $r_c = 1.61$ au, which corresponds to the expectation value of $\langle r \rangle$ for the outermost core orbital, i.e., 5d, as obtained with Cowan's code. A least-squares

Table 2
BFs, Transition Probabilities, and Oscillator Strengths Obtained in the Present Work for Highly Excited Levels of Ir II, and Comparison with Previous Results

Upper Level[a]		Lower Level[a]		λ[b] (nm)	BFs			gA (10^7 s^{-1})			Log(gf)	
Assign.	E (cm^{-1}) Life-time (ns)	Assign.	E (cm^{-1})		This Work[c]	Previous		This Work[f]	Previous		This Work[f]	Previous Exp.[d]
						Exp.[d]	Cal.[e]		Exp.[d]	Cal.[e]		
$5d^7(^4F_{9/2})6p$ $(9/2,1/2)^\circ_5$	47,003.95 $\tau = 4.1(3)$	$5d^7(^4F)6s$ $^5F_5$	0.00	212.681	0.736	0.688	0.738	197.44(C+)	172.07	189.74*	0.13 (C+)	0.07
		$5d^7(^4F)6s^5F_4$	4787.92	236.805	0.181	0.260	0.181	48.65 (E)	64.91	46.67*	−0.39 (E)	−0.26
		$5d^7(^4F)6s^3F_4$	11,719.11	283.325	0.064		0.064	17.10 (E)		16.40*	−0.69 (E)	
		$5d^6 6s^2$ $^5D_4$	19,279.04	360.584	0.011		0.011	2.88 (E)		2.76*	−1.25 (E)	
$5d^6 6s(^6D_{9/2})6p$ $(9/2,1/2)^\circ_4$	50,302.01 $\tau = 34(3)$	$5d^7(^4F)6s$ $^5F_5$	0.00	198.799	0.487	0.637	0.491	12.90 (C)	16.87	12.83*	−1.12 (C)	−1.00
		$5d^8$ $^3F_4$	2262.84	208.097	0.014		0.014	0.38 (E)		0.38*	−2.60 (E)	
		$5d^7(^4F)6s^5F_4$	4787.92	219.643	0.253	0.300	0.253	6.71 (D+)	7.93	6.63*	−1.31 (D+)	−1.24
		$5d^7(^4F)6s^5F_3$	8186.89	237.373	0.019		0.019	0.50 (E)		0.50*	−2.37 (E)	
		$5d^7(^4F)6s^3F_4$	11,719.11	259.105	0.053		0.053	1.40 (E)		1.39*	−1.85 (E)	
		$5d^7(^4P)6s^5P_3$	12,714.66	265.968	0.016		0.016	0.43 (E)		0.42*	−2.34 (E)	
		$5d^8$ $^1G_4$	17,210.16	302.101	0.052		0.052	1.37 (E)		1.35*	−1.73 (E)	
		$5d^7(^2G)6s$ $^3G_5$	17,477.99	304.565	0.038		0.038	1.01 (E)		1.01*	−1.85 (E)	
		$5d^6 6s^2$ $^5D_4$	19,279.04	322.249	0.047		0.047	1.23 (E)		1.22*	−1.72 (E)	
$5d^6 6s(^6D_{9/2})6p$ $(9/2,1/2)^\circ_5$	51,333.00 $\tau = 53(3)$	$5d^7(^4F)6s$ $^5F_5$	0.00	194.806	0.606	0.845	0.606	12.57 (C+)	17.87	12.82*	−1.15 (C+)	−0.99
		$5d^7(^4F)6s^5F_4$	4787.92	214.778	0.021		0.021	0.43 (E)		0.45*	−2.52 (E)	
		$5d^8$ $^1G_4$	17,210.16	292.973	0.214		0.215	4.45 (D+)		4.54*	−1.24 (D+)	
		$5d^6 6s^2$ $^5D_4$	19,279.04	311.884	0.133		0.133	2.75 (E)		2.81*	−1.40 (E)	
$5d^7(^4P_{5/2})6p$ $(5/2,1/2)^\circ_2$	51,371.97 $\tau = 6.6(4)$	$5d^8$ $^3P_2$	3090.16	207.051	0.154		0.154	11.63 (E)		11.71*	−1.13 (E)	
		$5d^7(^4F)6s^5F_3$	8186.89	231.491	0.288	0.250	0.288	21.78 (D+)	18.96	21.88*	−0.76 (D+)	−0.82
		$5d^8$ $^1D_2$	8974.95	235.794	0.161	0.146	0.161	12.16 (E)	11.07	12.23*	−0.99 (E)	−1.03
		$5d^7(^4P)6s^5P_3$	12,714.66	258.606	0.291	0.469	0.291	22.04 (D+)	35.54	22.14*	−0.66 (D+)	−0.45
		$5d^7(^4P)6s$ $^5P_2$	15,676.25	280.063	0.069		0.069	5.25 (E)		5.27*	−1.21 (E)	
		$5d^7(^4P)6s$ $^3P_2$	18,944.91	308.295	0.013		0.013	0.95 (E)		0.95*	−1.87 (E)	
$5d^7(^4F_{3/2})6p(3/2,1/2)^\circ_2$	53,678.68 τ = 6.3(10)	$5d^8$ $^3P_2$	3090.16	197.673	0.017		0.017	1.37 (E)		1.24	−2.10 (E)	
		$5d^7(^4F)6s^5F_3$	8186.89	219.751	0.501		0.502	39.79 (C)		36.13	−0.54 (C)	
		$5d^8$ $^1D_2$	8974.95	223.626	0.080		0.080	6.32 (E)		5.73	−1.32 (E)	
		$5d^8$ $^3P_1$	9062.22	224.062	0.041		0.041	3.28 (E)		2.98	−1.61 (E)	
		$5d^7(^4F)6s$ $^5F_2$	11,307.53	235.936	0.083		0.083	6.61 (E)		5.99	−1.26 (E)	
		$5d^7(^4F)6s$ $^5F_1$	11,957.83	239.615	0.017		0.017	1.38 (E)		1.25	−1.93 (E)	
		$5d^7(^4P)6s^5P_3$	12,714.66	244.043	0.059		0.059	4.70 (E)		4.26	−1.38 (E)	
		$5d^7(^4F)6s$ $^3F_3$	17,499.26	276.318	0.134		0.134	10.63 (E)		9.64	−0.91 (E)	
		$5d^7(^4P)6s$ $^3P_2$	18,944.91	287.820	0.013		0.013	1.01 (E)		0.91	−1.90 (E)	
		$5d^7(^4P)6s$ $^3P_1$	20,440.64	300.772	0.020		0.020	1.58 (E)		1.43	−1.67 (E)	
$5d^7(^4F_{9/2})6p$ $(9/2,3/2)^\circ_5$	53,691.38 $\tau = 3.4(3)$	$5d^7(^4F)6s$ $^5F_5$	0.00	186.250	0.314		0.315	101.55 (D+)		133.30	−0.28 (D+)	
		$5d^8$ $^3F_4$	2262.84	194.444	0.056		0.056	18.24 (E)		20.25	−0.99 (E)	
		$5d^7(^4F)6s^5F_4$	4787.92	204.419	0.494		0.495	159.97 (C)		178.10	0.00 (C)	
		$5d^7(^4F)6s^3F_4$	11719.11	238.179	0.111		0.111	35.86 (E)		39.93	−0.52 (E)	
		$5d^8$ $^1G_4$	17210.16	274.032	0.013		0.013	4.30 (E)		4.78	−1.32 (E)	

Table 2
(Continued)

Upper Level[a]		Lower Level[a]		λ[b] (nm)	BFs			gA (10^7 s^{-1})			Log(gf)	
Assign.	E (cm^{-1}) Life-time (ns)	Assign.	E (cm^{-1})		This Work[c]	Previous		This Work[f]	Previous		This Work[f]	Previous Exp.[d]
						Exp.[d]	Cal.[e]		Exp.[d]	Cal.[e]		
		$5d^7(^2\mathrm{H})6s\ ^3\mathrm{H}_6$	22,266.92	318.132	0.005		0.005	1.63 (E)		1.81	−1.61 (E)	
$5d^7(^4\mathrm{F}_{5/2})6p\ (5/2,1/2)^\circ_3$	55,852.5 $\tau = 5.8(3)$	$5d^8\ ^3\mathrm{F}_4$	2262.84	186.603	0.015		0.015	1.86 (E)		1.49	−2.01 (E)	
		$5d^7(^4\mathrm{F})6s^5\mathrm{F}_4$	4787.92	195.830	0.034		0.034	4.15 (E)		3.32	−1.62 (E)	
		$5d^7(^4\mathrm{F})6s^5\mathrm{F}_3$	8186.89	209.728	0.062		0.062	7.47 (E)		5.98	−1.31 (E)	
		$5d^8\ ^1\mathrm{D}_2$	8974.95	213.255	0.207		0.207	24.99 (D+)		20.04	−0.77 (D+)	
		$5d^8\ ^3\mathrm{F}_3$	9927.84	217.680	0.026		0.026	3.19 (E)		2.55	−1.64 (E)	
		$5d^7(^4\mathrm{F})6s\ ^5\mathrm{F}_2$	11,307.53.	224.421	0.045		0.045	5.47 (E)		4.38	−1.38 (E)	
		$5d^7(^4\mathrm{F})6s^3\mathrm{F}_4$	11,719.11	226.516	0.140		0.140	16.87 (E)		13.52	−0.89 (E)	
		$5d^7(^4\mathrm{P})6s^5\mathrm{P}_3$	12,714.66	231.744	0.133		0.132	15.99 (E)		12.77	−0.89 (E)	
		$5d^7(^4\mathrm{P})6s\ ^5\mathrm{P}_2$	15,676.25	248.829	0.094		0.094	11.36 (E)		9.09	−0.98 (E)	
		$5d^7(^4\mathrm{F})6s\ ^3\mathrm{F}_3$	17,499.26	260.656	0.093		0.093	11.24 (E)		9.00	−0.94 (E)	
		$5d^7(^4\mathrm{P})6s\ ^3\mathrm{P}_2$	18,944.91	270.867	0.095		0.095	11.43 (E)		9.15	−0.90 (E)	
		$5d^6 6s^2\ ^5\mathrm{D}_2$	25,563.67	330.060	0.014		0.014	1.65 (E)		1.32	−1.57 (E)	
$5d^7(^4\mathrm{F}_{9/2})6p\ (9/2,3/2)^\circ_4$	56,233.93 $\tau = 3.3(2)$	$5d^7(^4\mathrm{F})6s\ ^5\mathrm{F}_5$	0.00	177.829	0.127		0.127	34.70 (E)		28.45	−0.78 (E)	
		$5d^8\ ^3\mathrm{F}_4$	2262.84	185.284	0.060		0.060	16.31 (E)		13.37	−1.08 (E)	
		$5d^7(^4\mathrm{F})6s^5\mathrm{F}_4$	4787.92	194.379	0.111		0.111	30.32 (E)		24.93	−0.77 (E)	
		$5d^7(^4\mathrm{F})6s^5\mathrm{F}_3$	8186.89	208.064	0.084		0.084	23.01 (E)		18.93	−0.83 (E)	
		$5d^7(^4\mathrm{F})6s^3\mathrm{F}_4$	11,719.11	224.574	0.260		0.260	70.98 (D+)		58.29	−0.27 (D+)	
		$5d^7(^4\mathrm{P})6s^5\mathrm{P}_3$	12,714.66	229.712	0.063		0.063	17.05 (E)		14.01	−0.87 (E)	
		$5d^8\ ^1\mathrm{G}_4$	17,210.16	256.177	0.027		0.026	7.23 (E)		5.94	−1.15 (E)	
		$5d^7(^2\mathrm{G})6s\ ^3\mathrm{G}_5$	17,477.99	257.947	0.215		0.215	58.69 (D+)		48.15	−0.23 (D+)	
		$5d^6 6s^2\ ^5\mathrm{D}_4$	19,279.04	270.520	0.018		0.018	4.91 (E)		4.03	−1.27 (E)	
$5d^7(^4\mathrm{P}_{3/2})6p\ (3/2,1/2)^\circ_1$	56,241.53 $\tau = 8.5(4)$	$5d^8\ ^3\mathrm{P}_2$	3090.16	188.142	0.039		0.039	1.36 (E)		1.75	−2.14 (E)	
		$5d^8\ ^1\mathrm{D}_2$	8974.95	211.499	0.011		0.011	0.40 (E)		0.51	−2.57 (E)	
		$5d^8\ ^3\mathrm{P}_1$	9062.22	211.890	0.058		0.058	2.06 (E)		2.65	−1.86 (E)	
		$5d^7(^4\mathrm{F})6s\ ^5\mathrm{F}_2$	11,307.53	222.479	0.193		0.193	6.83 (D+)		8.75	−1.30 (D+)	
		$5d^7(^4\mathrm{F})6s\ ^5\mathrm{F}_1$	11,957.83	225.746	0.417		0.417	14.73 (C)		18.90	−0.95 (C)	
		$5d^7(^4\mathrm{P})6s\ ^5\mathrm{P}_2$	15,676.25	246.442	0.110		0.110	3.89 (E)		4.99	−1.45 (E)	
		$5d^8\ ^3\mathrm{F}_2$	17,413.25	257.467	0.038		0.038	1.33 (E)		1.71	−1.88 (E)	
		$5d^7(^4\mathrm{P})6s\ ^5\mathrm{P}_1$	18,676.49	266.126	0.051		0.051	1.82 (E)		2.32	−1.71 (E)	
		$5d^7(^4\mathrm{P})6s\ ^3\mathrm{P}_2$	18,944.91	268.041	0.020		0.020	0.69 (E)		0.89	−2.13 (E)	
		$5d^7(^4\mathrm{F})6s\ ^3\mathrm{F}_2$	22,467.78	296.002	0.035		0.035	1.23 (E)		1.58	−1.79 (E)	
$5d^6 6s(^6\mathrm{D}_{5/2})6p\ (5/2,1/2)^\circ_2$	56,354.21 $\tau = 9.3(3)$	$5d^7(^4\mathrm{F})6s^5\mathrm{F}_3$	8186.89	207.544	0.190			10.2 (D+)			−1.18 (D+)	
		$5d^8\ ^3\mathrm{F}_3$	9927.84	215.327	0.021			1.12 (E)			−2.11 (E)	
		$5d^7(^4\mathrm{F})6s\ ^5\mathrm{F}_1$	11,957.83	225.173	0.049			2.63 (E)			−1.70 (E)	
		$5d^7(^4\mathrm{P})6s^5\mathrm{P}_3$	12,714.66	229.079	0.570			30.66 (C)			−0.62 (C)	
		$5d^7(^4\mathrm{F})6s\ ^3\mathrm{F}_3$	17,499.26	257.291	0.049			2.63 (E)			−1.58 (E)	
		$5d^7(^4\mathrm{P})6s\ ^5\mathrm{P}_1$	18,676.49	265.330	0.044			2.36 (E)			−1.60 (E)	
		$5d^6 6s^2\ ^5\mathrm{D}_3$	23,727.67	306.410	0.021			1.16 (E)			−1.79 (E)	

Table 2
(Continued)

Upper Level[a]		Lower Level[a]		λ[b] (nm)	BFs			gA (10^7 s^{-1})			Log(gf)	
Assign.	E (cm^{-1}) Life-time (ns)	Assign.	E (cm^{-1})		This Work[c]	Previous		This Work[f]	Previous		This Work[f]	Previous Exp.[d]
						Exp.[d]	Cal.[e]		Exp.[d]	Cal.[e]		
		$5d^6 6s^2\ ^5D_2$	25,563.67	324.682	0.015			0.80 (E)			−1.90 (E)	
5664°$_2$	56,644.46 $\tau = 4.6(4)$	$5d^7(^4F)6s^5F_3$	8186.89	206.300	0.018			1.92 (E)			−1.91 (E)	
		$5d^8\ ^1D_2$	8974.95	209.711	0.103			11.16 (E)			−1.13 (E)	
		$5d^8\ ^3P_1$	9062.22	210.095	0.116			12.60 (E)			−1.08 (E)	
		$5d^7(^4F)6s\ ^5F_2$	11,307.53	220.501	0.419			45.59 (C)			−0.48 (C)	
		$5d^7(^4F)6s\ ^5F_1$	11,957.83	223.711	0.186			20.20 (D+)			−0.82 (D+)	
		$5d^7(^4P)6s\ ^5P_2$	15,676.25	244.018	0.058			6.33 (E)			−1.25 (E)	
		$5d^7(^4F)6s\ ^3F_3$	17,499.26	255.382	0.019			2.10 (E)			−1.69 (E)	
		$5d^7(^4P)6s\ ^3P_2$	18,944.91	265.176	0.021			2.33 (E)			−1.61 (E)	
		$5d^7(^4F)6s\ ^3F_2$	22,467.78	292.511	0.033			3.56 (E)			−1.34 (E)	
$5d^7(^4P_{1/2})6p$ (1/2,1/2)°$_0$	56,875.79 $\tau = 5.5(3)$	$5d^8\ ^3P_1$	9062.22	209.079	0.728		0.728	13.23 (C+)		14.68	−1.06 (C+)	
		$5d^7(^4P)6s\ ^5P_1$	18,676.49	261.707	0.197		0.197	3.58 (D+)		3.98	−1.43 (D+)	
		$5d^7(^4P)6s\ ^3P_1$	20,440.64	274.379	0.060		0.060	1.09 (E)		1.20	−1.91 (E)	
$5d^7(^4P_{3/2})6p$ (3/2,1/2)°$_2$	59,132.98 $\tau = 5.9(3)$	$5d^8\ ^3P_2$	3090.16	178.435	0.022		0.022	1.85 (E)		1.74	−2.06 (E)	
		$5d^7(^4F)6s^5F_3$	8186.89	196.286	0.146		0.146	12.41 (E)		11.68	−1.14 (E)	
		$5d^8\ ^1D_2$	8974.95	199.370	0.185		0.186	15.7 (D+)		14.81	−1.03 (D+)	
		$5d^8\ ^3P_1$	9062.22	199.717	0.303		0.303	25.67 (D+)		24.20	−0.81 (D+)	
		$5d^8\ ^3F_3$	9927.84	203.166	0.056		0.056	4.74 (E)		4.47	−1.53 (E)	
		$5d^7(^4F)6s\ ^5F_2$	11,307.53	209.027	0.045		0.046	3.85 (E)		3.63	−1.60 (E)	
		$5d^7(^4F)6s\ ^5F_1$	11,957.83	211.908	0.047		0.047	3.99 (E)		3.75	−1.57 (E)	
		$5d^7(^4F)6s\ ^3F_3$	17,499.26	240.117	0.060		0.060	5.08 (E)		4.79	−1.36 (E)	
		$5d^8\ ^3F_2$	17,413.25	239.622	0.014		0.014	1.21 (E)		1.14	−1.98 (E)	
		$5d^7(^4P)6s\ ^3P_2$	18,944.91	248.755	0.020		0.020	1.69 (E)		1.59	−1.81 (E)	
		$5d^7(^4F)6s\ ^3F_2$	22,467.78	272.657	0.012		0.012	1.00 (E)		0.94	−1.95 (E)	
		$5d^6 6s^2\ ^5D_1$	28,600.34	327.424	0.010		0.010	0.85 (E)		0.80	−1.86 (E)	
$5d^7(^4F_{9/2})6p$ (9/2,3/2)°$_3$	60,313.63 $\tau = 3.4(3)$	$5d^8\ ^3F_4$	2262.84	172.263	0.055			11.32 (E)			−1.30 (E)	
		$5d^7(^4F)6s^5F_4$	4787.92	180.097	0.013			2.68 (E)			−1.89 (E)	
		$5d^7(^4F)6s^5F_3$	8186.89	191.840	0.302			62.18 (D+)			−0.46 (D+)	
		$5d^8\ ^1D_2$	8974.95	194.785	0.125			25.74 (E)			−0.83 (E)	
		$5d^7(^4F)6s^3F_4$	11,719.11	205.719	0.244			50.24 (D+)			−0.50 (D+)	
		$5d^7(^4P)6s\ ^5P_2$	15,676.25	223.958	0.027			5.56 (E)			−1.38 (E)	
		$5d^7(^4F)6s\ ^3F_3$	17,499.26	233.495	0.062			12.76 (E)			−0.98 (E)	
		$5d^7(^4P)6s\ ^3P_2$	18,944.91	241.655	0.020			4.12 (E)			−1.44 (E)	
		$5d^7(^2G)6s\ ^3G_4$	20,294.25	249.804	0.062			12.76 (E)			−0.92 (E)	
		$5d^6 6s^2\ ^5D_3$	23,727.61	273.248	0.028			5.76 (E)			−1.19 (E)	
6147°$_3$	61,474.19 $\tau = 3.9(3)$	$5d^8\ ^3F_4$	2262.84	168.886	0.032			5.73 (E)			−1.61 (E)	
		$5d^8\ ^3P_2$	3090.16	171.280	0.262			47.06 (D+)				

Table 2
(Continued)

Upper Level[a]		Lower Level[a]		λ[b] (nm)	BFs			gA (10^7 s^{-1})			Log(gf)	
Assign.	E (cm^{-1}) Lifetime (ns)	Assign.	E (cm^{-1})		This Work[c]	Previous		This Work[f]	Previous		This Work[f]	Previous Exp.[d]
						Exp.[d]	Cal.[e]		Exp.[d]	Cal.[e]		
											−0.68 (D+)	
		$5d^7(^4\mathrm{F})6s\,^5\mathrm{F}_3$	8186.89	187.662	0.030			5.41 (E)			−1.54 (E)	
		$5d^7(^4\mathrm{F})6s\,^5\mathrm{F}_2$	11,307.53	199.335	0.092			16.59 (E)			−1.01 (E)	
		$5d^7(^4\mathrm{F})6s\,^3\mathrm{F}_4$	11,719.11	200.919	0.022			3.99 (E)			−1.62 (E)	
		$5d^7(^4\mathrm{P})6s\,^5\mathrm{P}_3$	12,714.66	205.022	0.142			25.46 (E)			−0.79 (E)	
		$5d^7(^4\mathrm{P})6s\,^5\mathrm{P}_2$	15,676.25	218.283	0.122			21.81 (E)			−0.81 (E)	
		$5d^8\,^1\mathrm{G}_4$	17,210.16	225.847	0.104			18.68 (E)			−0.84 (E)	
		$5d^8\,^3\mathrm{F}_2$	17,413.25	226.888	0.077			13.77 (E)			−0.97 (E)	
		$5d^7(^4\mathrm{P})6s\,^3\mathrm{P}_2$	18,944.91	235.060	0.033			5.91 (E)			−1.31 (E)	
		$5d^6 6s^2\,^5\mathrm{D}_4$	19,279.04	236.922	0.013			2.34 (E)			−1.71 (E)	
		$5d^7(^4\mathrm{F})6s\,^3\mathrm{F}_2$	22,467.78	256.291	0.026			4.74 (E)			−1.33 (E)	

Notes.
[a] Kramida et al. (2020).
[b] Wavelengths above 200 nm are listed as air wavelengths and below as vacuum wavelengths.
[c] BFs calculated using the HFR+CPOL method.
[d] Ivarsson et al. (2004).
[e] Xu et al. (2007). The gA values marked with an asterisk (*) were obtained by combining the experimental lifetimes with the theoretical BFs.
[f] gA and log gf values obtained in this work were deduced from the combination of HFR+CPOL BFs with experimental lifetimes. The estimated uncertainties are given in parentheses. They are indicated by the same code letter as the one used in the NIST database (Kramida et al. 2020), i.e., B (⩽10%), C+ (⩽18%), C (⩽25%), D+ (⩽40%), D (⩽50%) and E (>50%) (see text).

optimization process minimizing the discrepancies between the calculated eigenvalues and experimental energy levels published by Van Kleef & Metsch (1978), and now compiled in the NIST database (Kramida et al. 2020) was then carried out. Compared to Xu et al.'s work, which was limited to the odd levels below 60,000 cm^{-1}, two additional levels were introduced in the semiempirical process of our study, namely the levels located at 60,313.63 cm^{-1} ($J = 3$) and 61,474.19 cm^{-1} ($J = 3$), for which we measured new experimental radiative lifetimes. For the latter, our calculations gave 59,932 and 61,152 cm^{-1}, respectively. These levels also appeared extremely mixed in our calculations insofar as their main components in LS coupling were found to be equal to 16% $5d^6(^5D)6s6p\ ^7F_3$ for the first one and 24% $5d^7(^4P)6p\ ^5P_3$ for the second one.

4. Results and Discussion

The lifetimes measured in the present work for 15 odd-parity levels of Ir II in the region of 47,003 to 61,475 cm^{-1} are listed in Table 1. The radiation lifetimes of 11 out of 15 of these energy levels were measured for the first time. For the four levels reported in the literature, our measurement results are in good agreement with the previous results by Ivarsson et al. (2004) and Xu et al. (2007). In the exponential fittings, for each fluorescence curve two lifetime values were determined with two starting points, one of which was chosen at a position just outside the affected region of the stray light of the exciting laser, and the other of which was at a position with half the intensity of the former point. In the deconvolution procedure, two lifetime values were also evaluated using two excitation pulses recorded before and after the registration of the corresponding fluorescence signal. The average of the two lifetime values was taken as the lifetime result revealed by this decay curve and the difference between them as the systematic error. The standard deviation of the systematic errors from all the curves recorded under different conditions for a level was taken as the systematic uncertainty of the final lifetime result. The systematic error reflects the uncertainty from the transit time jitter of the PMT (1.2 ns), the intensity nonlinear response of the whole detection system, the fluctuation of the exciting laser, etc. For each level, about 10 curves were recorded under different experimental conditions. The average value of the lifetimes evaluated from these curves was regarded as the final lifetime result with the corresponding standard deviation as the statistical error. The final uncertainties of the lifetime values consist of systematic errors and statistical errors from different recordings. Most of the uncertainties of our measurement results are less than 10%, and there is only one energy level with an uncertainty of 16%. The theoretical values obtained in the present work using the pseudorelativistic Hartree–Fock method without (HFR) and with (HFR+CPOL) core-polarization effects are also given in Table 1. A very good agreement between HFR +CPOL and experimental data is observed, the mean ratio $\tau_{HFR+CPOL}/\tau_{Exp}$ being found to be equal to 1.05 ± 0.14 for the 15 levels considered. The importance of core-polarization contributions is also obvious when examining this table since the HFR+CPOL lifetimes appear systematically about 30%–40% larger than the HFR values.

The BFs, transition probabilities gA, and oscillator strengths in the logarithmic scale $\log(gf)$ for highly excited levels of Ir II are listed in Table 2 along with previously reported results for comparison. The results of BFs determined by the HFR+CPOL model were combined with our experimental lifetimes to deduce the gA and $\log(gf)$ for all transitions with BF > 0.01 by the relations $A_{ik} = BF_{ik}/\tau_i$ and $g_kf = 1.4992 \times 10^{-16}\ \lambda^2 g_i A_{ik}$, where i and k represent the upper and lower levels, respectively; τ_i is the measured lifetime; λ is in units of angstroms and A_{ik} in s^{-1}, and g_i and g_k are the statistical weights of the upper and lower levels, respectively. Ivarsson et al. (2004) experimentally measured BFs and transition probabilities for eight transitions that were also investigated in the present work, and our results are in agreement within 40%. The uncertainties affecting our gA and gf values were estimated by combining experimental lifetime uncertainties with those evaluated for theoretical BF calculations, the latter being determined using the same procedure as the one considered in many of our previous works on Ir I (Zhou et al. 2018), Ba I (Wang et al. 2019), Rh I(Li et al. 2021), and Nb II (Geng et al. 2021). As a reminder, in these works we noticed a rather regular pattern of increasingly deviating weak BFs when comparing the calculated HFR+CPOL values with available experimental measurements. More precisely, the average uncertainties on computed BF values were systematically found to be about 10%–20% for $0.8 < BF < 1.0$, 20%–30% for $0.6 < BF < 0.8$, 30%–40% for $0.4 < BF < 0.6$, 40%–50% for $0.2 < BF < 0.4$, and 50%–100% for $0.0 < BF < 0.2$. It is interesting to note that the uncertainties follow a trend which can be roughly approximated by a simple formula of the type $0.2/BF_{max}$ regardless of the BF range mentioned above, for which BF_{max} is the maximum of each BF range. These uncertainties were then combined in quadrature with the experimental lifetime uncertainties derived from our measurements to yield the uncertainties of gA and gf values. For simplicity, the uncertainties on the final results listed in Table 2 are given using the same letter coding as the one used in these latter papers, inspired by the one usually employed in the NIST database (Kramida et al. 2020), i.e., B (=10%), C (=25%), $D+$ (=40%), D (=50%), and E (>50%).

The radiative parameters presented in this work largely supplement the radiative data of the Ir II ion especially for highly excited states, which are of great significance for understanding the transition dynamics properties and astronomical spectral analyses of this ion.

This work was supported by the National Natural Science Foundation of China (grant No. U1832114). P.Q. is the Research Director of the Belgian Fund for Scientific Research (F.R.S.-FNRS) from which financial support is greatly appreciated.

ORCID iDs

Zhenwen Dai https://orcid.org/0000-0002-9040-2315

References

Biémont, E., & Quinet, P. 2003, PhST, T105, 38
Cowan, R. D. 1981, The Theory of Atomic Structure and Spectra (Berkeley, CA: Univ. California Press)
Cowan, J. J., Sneden, C., Truran, J. W., & Burris, D. L. 1996, ApJ, 460, L115
Cowley, C. R., Ayres, T. R., Castelli, F., et al. 2016, ApJ, 826, 158
Fraga, S., Karwowski, J., & Saxena, K. M. S. 1976, Handbook of Atomic Data (Amsterdam: Elsevier)
Frebel, A. 2018, ARNPS, 68, 237
Geng, Y. D., Liu, Y., Zheng, H. F., et al. 2021, ApJS, 259, 44
Ivarsson, S., Wahlgren, G. M., Dai, Z., Lundberg, H., & Leckrone, D. S. 2004, A&A, 425, 353

Kramida, A., Ralchenko, Yu., Reader, J. & NIST ASD Team 2020, NIST Atomic Spectra Database (Gaithersburg, MD: National Institute of Standards and Technology), https://physics.nist.gov/asd
Li, Z. S., Norin, J., Persson, A., Wahlström, C. G., & Svanberg, S. 1999, PhRvA, 60, 198
Li, Y. F., Geng, Y. D., Liu, M. N., et al. 2021, MNRAS, 503, 5085
Quinet, P. 2017, CaJPh, 95, 790
Quinet, P., Palmeri, P., Biémont, E., et al. 1999, MNRAS, 307, 934
Quinet, P., Palmeri, P., Biémont, E., et al. 2002, J. Alloys Compd., 344, 255
Roederer, I. U., & Lawler, J. E. 2012, ApJ, 750, 76
Sneden, C., Cowan, J. J., Burris, D. L., & Truran, J. W. 1998, ApJ, 496, 235
Tian, Y. S., Wang, X. H., Yu, Q., et al. 2016, MNRAS, 457, 1393
Van Kleef, Th. A. M., & Metsch, B. C. 1978, PhyBC, 95, 251
Wang, Q., Gamrath, S., Palmeri, P., et al. 2019, JQSRT, 225, 35
Wahlgren, G. M., Nielsen, K. E., & Leckrone, D. S. 2021, MNRAS, 500, 2451
Xu, H. L., Svanberg, S., Quinet, P., Palmeri, P., & Biémont, E. 2007, JQSRT, 104, 52
Zhou, L. N., Gamrath, S., Palmeri, P., et al. 2018, ApJS, 238, 3